Contents lists available at ScienceDirect

Materials & Design

Smart Milli-capsules manipulated by nIR irradiation for controllable drug delivery in-vivo for renal cell carcinoma and neurodegenerative diseases

Rui Jia [a,1], Tian Li [b,1], Weitao Jiang [b,c,d,*], Jing Wang [e], Xiao Li [f], Qiumin Qu [a], Jingxia Dang [a], Pingping Li [f,*]

[a] Department of Neurology, The First Affiliated Hospital of Xi'an Jiaotong University, Xi'an 710061, China
[b] State Key Laboratory for Manufacturing Systems Engineering, Xi'an Jiaotong University, Xi'an 710049, China
[c] Shaanxi Joint Key Laboratory of Graphene, Xi'an 710049, China
[d] Xi'an Key Laboratory of trans-scale standard measurement, Xi'an 710049, China
[e] Department of Rheumatology and Immunology, The First Affiliated Hospital of Xi'an Jiaotong University, Xi'an 710061, China
[f] Center for Translational Medicine, The First Affiliated Hospital of Xi'an Jiaotong University, Xi'an 710061, China

HIGHLIGHTS

- nIR lights in vitro and GO-based milli-capsules in vivo have higher matching score to realize desired on/off drug-dosing.
- Light powers, GO-concentrations and structural dimensions of photo-triggered switches directly affect the drug release.
- Milli-capsules inhibit ccRCC cells proliferation in a GO-concentration-dependent manner by accurate GO-dosing control.
- Capsules applications in neurodegeneration was popularized by embed siRNA-drugs which inhibit autophagy in NSC-34 neurons.

GRAPHICAL ABSTRACT
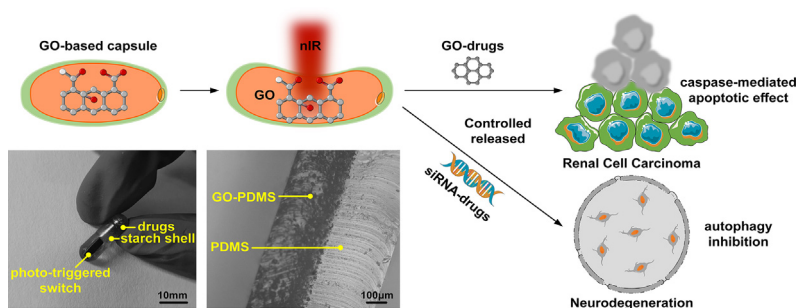
ARTICLE INFO

ABSTRACT

Cancer and neurodegeneration which are responsible for million deaths worldwide, have urgent requests for drug administration with little to no side-effects. Current designs of drug-delivery, however, are constrained by either treatment effectiveness caused by imprecise control of drug-concentrations, or treatment-related toxicities caused by drugs-themselves or drug-carrier-systems, as well as the safety and feasibility. In this study, on account of the penetration ability through tissues of near-infrared (nIR) lights and the nIR-absorption ability of graphene oxide (GO), the GO-based milli-capsule is constructed, with controlled drug release ability by photomechanical deformation and wireless nIR manipulation. When radiation powers increasing from 0.1 to 0.5 W, drug dosages are in the range of 0 μg (0 drop) to 225 μg (five drops). The cytotoxicity of GO-based capsules in vitro is evaluated by embedded GO as drugs and released GO in clear cell renal cell carcinoma (ccRCC). When the capsules irradiated under 0.5 W and released different amounts of GO-drops in ccRCC, GO-concentrations increase from 0 to 80 μg·mL^{-1} and the proportions of apoptotic cells increase 2.85 times, which proves milli-capsules inhibit ccRCC cells proliferation in a GO-concentration-dependent manner by accurate GO-dosing control. Other drugs such as siRNA furnishing an additional practicability-proof for neurodegeneration therapy.

* Corresponding authors.
  E-mail addresses: wtjiang@mail.xjtu.edu.cn (W. Jiang), lipingping@xjtu.edu.cn (P. Li).
[1] Equal contribution to this work.

1. Introduction

Neurodegenerative diseases and cancer, which caused by neurons death or failed to stop uncontrolled cells pathological growth, are the major two causes of death worldwide. Renal cell carcinoma (RCC) as the most common type of kidney cancer in men aged over 65,[1,2] its histologic subtype clear cell RCC (ccRCC) accounts for approximately 90 % of kidney cancers and 4 % of all newly diagnosed cancer cases.[3] Since RCC is usually asymptomatic, few patients are diagnosed at initial clinical assessment until symptoms develop secondary to serious kidney damage. For patients with a localized disease in the kidney, approximately 70–80 % of patients undergo nephrectomy to remove the tumor and the recurrence rate is usually<25 % (surgery alone might achieve adequate curing). For patients with advanced cancer (i.e. tumor has spread outside the kidney), however, the recurrence rate is up to 40 % after initial treatment,[4,5] and the five-year survival rate is still much lower (12 %).[6] In addition, some neurodegenerative diseases, such as Alzheimer's Disease (AD), Amyotrophic Lateral Sclerosis (ALS) and Parkinson's Disease (PD), are facing challenges in pathogenesis and treatment,[7] also due to their insidious onset and nonspecific symptoms at different developmental stages.

Conventional kidney cancer treatments (include chemo- and radiotherapy) met the bottlenecks caused by increased resistance of RCC, therefore, modern cancer therapies were pursuing similar approaches to create methods that were more specific and had fewer unwanted side effects on healthy cells. For example, targeted therapies are directly designed to pathogenic cells and killing only tumor cells, immunotherapies work by restoring the function of the innate anticancer immune system.[8–11] Nowadays, drug-delivery devices which meet specified dosing challenges have attained great attention. For conventional oral and parenteral drug delivery systems,[23] passive tumor targeting are prone to obtain sub-therapeutic response due to the difficulty of maintaining plasma drug concentrations above the minimum effective value and below the toxic level simultaneously.[20] For example, PEG-based systems released drug dependent on advanced prodrugs, which obtained optimum therapies constrained by rapid drug elimination.[36] For state-of-art implantable drug delivery systems,[24–27] active tumor targeting based on stimuli-responsive strategies could maintain drug levels within the therapeutic window constantly and more likely to offer the desired therapeutic effect with a pre-determined duration.[21,22]. For example, temperature-responsive systems released drug by thermally degrade [37] or reversible shrinking [38] of the pump diaphragm, have dependence on favorable physiological conditions. [39,40] Magnetic-drug delivery systems required sufficient strength to deformed the membrane and modulated apertures scaling to control the release, [41] have hidden dangers in residual-magnetism retaining [42] and difficult to refilled drug in the reservoir.[23] Electric-responsive systems often realized wireless drug-release inseparable from electrical power sources, tended to result lower tissue penetration and biodegradability. [43,44] Light-stimuli as a wireless power source render systems delivery without motor to achieve the smallest size and lowest weight, [45]however, lower matching score may not be tolerated by the tissue and hard to achieve the desired therapeutic. e.g. The stimuli by visible or UV light are strongly limited to the skin or the mucosa treatment because their penetration depth into tissues could be no more than ~10 mm, and prolonged UV irradiation can be cytotoxic.[31].

Recently, the combination of biologically active compounds and carbon nanomaterials indicates a promising prospect in the biomedical field,[12,13] also provides new therapeutic strategies for stimuli-responsive systems realize implantable drug delivery. Graphene oxide (GO), since they possess high surface-to-volume ratio and demonstrate cytotoxic effect on several human cancer cell lines (e.g. osteosarcoma,[14] A549 lung cancer,[15] and ovarian cancer [16]), render themselves attractive candidates for drug delivery.[17–19] Although much progress evaluate the toxicity of GO in vitro have displayed extraordinary potential, there has been little discussion of GO-based drug delivery and some restrictions still exist in drugs' dosing accuracy and controllability, as well as implantable delivery and safety. In addition to ccRCC, neurodegenerative diseases, which need to observe the progression when administrate new drugs and compare effectiveness of animal-models with different dosages, also have an urgent request for accurate drug-dosing control of delivery devices.[7].

In this study, on account of the penetration ability through tissues of near-infrared (nIR) lights and the nIR absorption ability of graphene oxide (GO), we construct a GO-based milli-capsule composed of the capsule shell and photo-triggered switch. As Fig. 1 shows, the switches' photomechanical deformations could be utilized as an alternative electric power source, which is beneficial to the minimization of drug-release capsules. It could be found that, the ability of controllable drug-release depends on the reversible deformation by the remote nIR irradiation ("on" or "off" in controllable manner), and the capsules could be re-used after refiled. Capsules' cytotoxicity in vitro are evaluated by embedded with GO as drugs and released GO in clear cell renal cell carcinoma (ccRCC), where dosage controlled in the range of 0 μg (0 drop) to 225 μg (five drops) when the radiation power increased from 0.1 to 0.5 W. Drugs' caspase-mediated apoptotic effect on ccRCC cell lines increased 2.85 times compared with pure ccRCC when the GO-concentration increased to 80 $\mu g \cdot mL^{-1}$ (capsules irradiated under 0.5 W and released four GO-drops in 2.25 mL nutrient solution). The proposed GO-based milli-capsules were finally implanted under the skin of live mice in vivo, further evaluates the validity of our drug delivery systems in physiological tissues, and provides feasible paths for ccRCC therapy and neurodegeneration therapy by embedded with corresponding drugs.

2. Materials and methods

2.1. Materials and micro-fabrication of GO-based capsules

Starch shells were purchased from Hunan ER-Kang Pharmaceutical Limited by Share ltd, the overall closed length is 21.70 ± 0.30 mm, and the volume capacity is 680 μL. GO nanosheets in the photo-triggered switch were purchased from Shenzhen Suiheng Technology Co. ltd, they are 1–10 μm in diameter and 1 nm in thickness in their original form. PDMS were obtained from Dow Corning (Sylgard 184).

PDMS layer was prepared by mixing the base component and the curing agent in a 10:1 ratio and followed with vacuum degassing, then spin-coated on a cleaned glass slides (500 rpm, 12 s) and cured at 100 °C for 60 min. GO-PDMS layer was obtained by weighting desired amount of GO and adding to liquid PDMS (the GO concentration was 5 wt% in this study), after thorough stirring and degasing, poured liquid GO-PDMS composites into the prefabricated mould (square border-shape); excess composites were
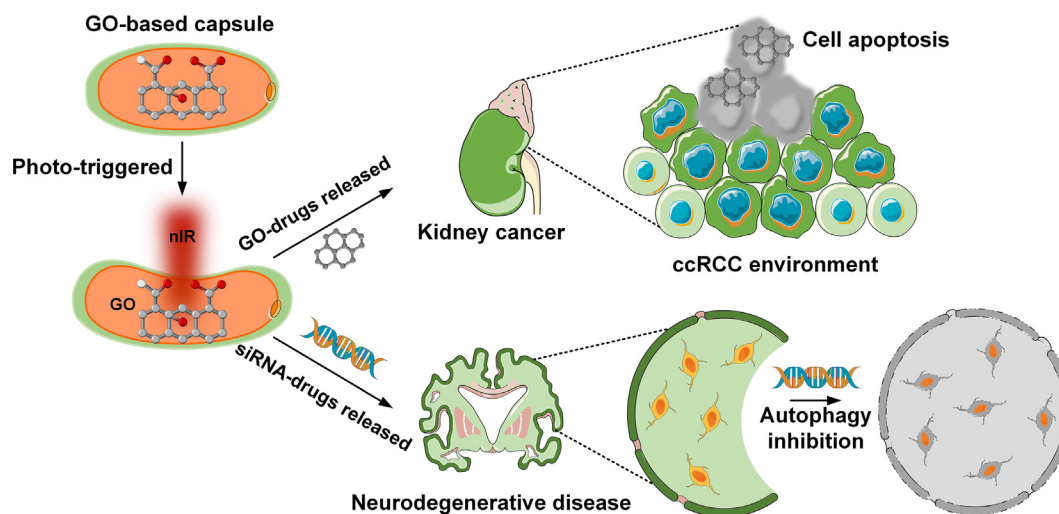
Fig. 1. Demonstration of the GO-based capsules with controlled drug released ability by remote nIR manipulation for implantable ccRCC or neurodegeneration therapy.

scraped by a doctor blade, remaining composites were cured at 100 °C for 60 min; then the mould was removed, and the GO-PDMS layer was fabricated on the pristine PDMS layer. The starch shell's top and side surfaces had a precast groove (5 mm × 1 mm) and a capillary hole (diameter<1 mm), the photo-triggered switch was bonding to the groove with PDMS in an uncured state, and then cured at room temperature for 12 h. GO or siRNA-drugs were first introduced into a syringe, before the needle inserted into the capillary hole on starch shells' side surfaces, flicked the side of the syringe and forced air bubbles up toward the needle hub, then gently pushed down the plunger to get the collected air out of the needle.

2.2. Materials and preparations for drugs

GO as drugs were purchased from Nanjing XFNANO Materials Tech Co. ltd (Nanjing, China). GO samples (XF020) were dispersed in pure water (1 $\mu g \cdot \mu L^{-1}$) as the stock solution, and then the suspensions were autoclaved before starting the injection session. siRNA oligonucleotides as drugs for Beclin-1 (5′-CAGTTTGGCA CAATCAATATT-3′, 5′-UAUUGAUUGUGCCAAACUGTT-3′) and the control groups (5′-UUCUCCGAACGUGUCACGUTT-3′, 5′-ACGUGA CACGUUCGGAATT-3′) were synthesized by GenePharma (Shanghai, China).

2.3. Characterization of GO-based capsules

The thickness measurement of each layer contains three steps: (i) The prepared sample was cut perpendicularly to expose its cross-section, and mounted in a housing to ensure the cross-section perfectly under microscope; (ii) Optical microscopy was employed to obtain over 5 pictures of the pristine PDMS and GO-PDMS due to the sample have dimensions in microns and sufficiently high contrast. (iii) By the pictures, the average thickness of PDMS and GO-PDMS layer were calculated, which were 336 ± 2.82 μm and 283 ± 1.43 μm, respectively.

2.4. Controlled-release for desired drug-concentration

The desired GO-concentration c in the culture dish could controlled by the drug dosage m released from capsules and volume of nutrient solution V_n, i.e. $c = c(m, V_n)$, where light powers P_L can directly influence m, i.e. $m = m(P_L)$. As Table 1 shows, when cap-

sules irradiated under 0.5 W, different amount of GO (μg) released in various volume of nutrient solutions (mL) could realize desired GO-concentrations. i.e. 5 $\mu g \cdot mL^{-1} \sim 80$ $\mu g \cdot mL^{-1}$ (where $c = m/V_n$, the droplet's dropping volume (μL) is negligible compared to V_n). For 225 μL siRNA-drugs, capsules are irradiated under 0.5 W and released five drops.

2.5. Cell culture

Human ccRCC cell lines (Caki-1 and Caki-2) and 293 T cells (Human embryonic kidney cells) were obtained from the National Infrastructure of Cell Line Resource (Beijing, China). Caki-1 and Caki-2 were cultured in the recommended McCoy'5A Media (Hyclone, Logan, UT, USA) supplemented with 10 % FBS (Hyclone, USA). 293 T cells were cultured in H-DMEM (Gibco, 11965–092) with 10 % FBS. NSC-34 cell lines were obtained from the Otwo Biotech Inc. (Shenzhen, China), cultured in H-DMEM with 10 % FBS and 1 % Penicillin-Streptomycin (Gibco, 15070–063). All cells were maintained in a humidified incubator containing 5 % CO_2 at 37℃. All cell culture experiments performed standardized procedures, which are provided by National Infrastructure of Cell line Resources and Basic Biological and Medical Research or corresponding cell culture instructions (Website shown in Supporting Information I).

2.6. siRNA-drugs transfections on NSC-34 cells

NSC-34 cells were seeded into 6-well plates at a density of 5 × 10^5 per well and cultured for 24 h. NSC-34 cells were transfected with 225 μL (five drops) Beclin-1 or control siRNA transfection mixed liquid for 24 h. The Beclin-1 or control siRNA transfection mixed liquid were made by 20 μL Beclin-1 or control siRNA (concentration was 20 μM), 400 μL opti-MEM and 10 μL Lipofectamine™2000 (Invitrogen, 11668027) according to the instructions.

Limited by the article length, *Materials and Methods* of ccRCC cells viability assay, Cell apoptosis assay, Western blot assay and Statistical analysis shows in Supporting Information I.

Table 1
Preparation for desired GO-concentration, i.e. $c = c(m, V_n)$.

V_n	c m	45 ± 1 µg (one drop)	90 ± 1 µg (two drops)	135 ± 1 µg (three drops)	180 ± 1 µg (four drops)	225 ± 1 µg (five drops)
P_L	5 µg·mL^{-1}	9 mL	18 mL	27 mL	36 mL	45 mL
0.5 W	10 µg·mL^{-1}	4.5 mL	9 mL	13.5 mL	18 mL	22.5 mL
	20 µg·mL^{-1}	2.25 mL	4.5 mL	6.75 mL	9 mL	11.25 mL
	40 µg·mL^{-1}	1.125 mL	2.25 mL	3.375 mL	4.5 mL	5.625 mL
	80 µg·mL^{-1}	0.56 mL	1.125 mL	1.688 mL	2.25 mL	2.813 mL

3. Results and discussion

3.1. Design and fabrication of graphene Oxide-based milli-capsules.

The GO-based milli-capsule is constituted by the GO-based photo-triggered switch, the starch shell and built-in drugs, as Fig. 2a shows. The photo-thermal switch is a two-layer planar composite film based on the bimetallic strip effect, the upper layer is graphene oxide-polydimethylsiloxane nanocomposites (GO-PDMS) and the bottom layer is pristine PDMS, as Fig. 2b shows. The deformation of photo-thermal switch offers varying pressure to drive drug displacement as shown in Fig. 2c. When the developed switch fixed by PDMS solution on the starch shell and then spontaneous cured after 12 h, the GO-based milli-capsules finished its preparation as Fig. 2d shows. Different drugs such as GO or siRNA could embed in capsules for different disease therapy.

3.2. Controlled drug release of graphene Oxide-based milli-capsules

3.2.1. Drug-released mechanism for GO-based capsules

nIR lights as pressure source in vitro and GO as nIR- absorption source in vivo provide a feasible path to realize implantable drug delivery. When capsules irradiated under 808 nm nIR light, heat transfer rates dT/dt were calculated by eq. (1), temperature changes of photo-triggered switches T_{switch} and capsule-shells T_{capsule} were respectively demonstrated in Fig. 3a and b, where the switches have same thicknesses (h = 619 µm) and GO-concentrations (w_{GO} = 5 wt%). A is the spot area of the light, C_E is the volume heat capacity, defined as the amount of heat energy sample needed to raise one unit of temperature in per unit of volume.

$$\frac{dT}{dt} = \frac{P_L}{A \times C_E \times h} \tag{1}$$

When the nIR light irradiated on the switch (t = 10 s), T_{switch} increased rapidly in 10 s, while $T_{\text{capsule-n}}$ (temperature of the capsule-shell near to the switch) increased slowly, and $T_{\text{capsule-f}}$ (temperature of the capsule-shell far from the switch) experienced near-zero growth. When the nIR light stop irradiated (t = 40 s), T_{switch} decreased rapidly in 5 s, while $T_{\text{capsule-n}}$ and $T_{\text{capsule-f}}$ had continued growth in 5 s. Furthermore, final temperatures increased with light powers P_L and the maximum temperatures obtained at 0.5 W. The light power dependence of temperature changes illustrated that the temperature rise of the switch could attributed to the nIR light absorption of GO-PDMS and the conversion to thermal energy, and the capsule-shell temperature shows insignificant rise (<9 °C) due to heat conduction by switch.

Switches absorb thermal energy could further results photo-thermal deformations based on the bimetallic strip effect. Due to the component layers (i.e. GO-PDMS layer and pristine PDMS layer) have difference in thermal expansion α and elastic modulus E, switches could bend to the one side and induce deformations as eq. (2) shows.

$$\frac{1}{\rho} = \frac{6\Delta T(\alpha_{\text{PDMS}} - \alpha_{\text{GO - PDMS}})(1 + m^2)}{h[3(1 + m)^2 + (1 + mn)(m^2 + \frac{1}{mn})]} \tag{2}$$

Where $1/\rho$ is the deformation curvature of the photo-thermal switch, ΔT is the temperature difference, α is the coefficient of thermal expansion, m and n are the ratio of double layers' thickness ($m = h_{\text{GO-PDMS}}/h_{\text{PDMS}}$) and elastic modulus ($n = E_{\text{GO-PDMS}}/E_{\text{PDMS}}$), respectively. Eq. (2) shows that deformation $1/\rho$ is influenced by the differences in thermal properties (α, E and n) and structural
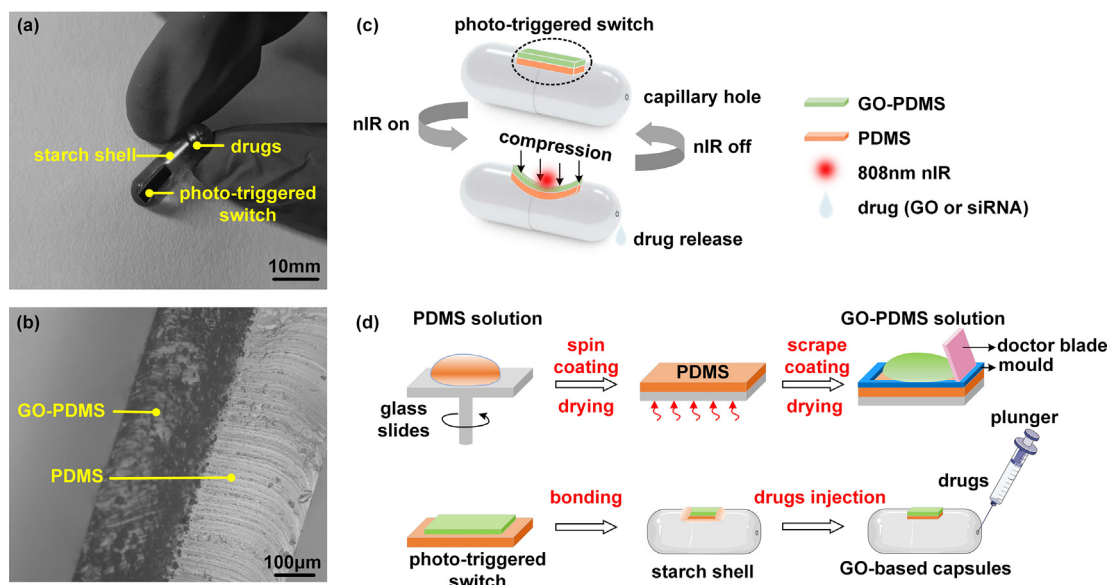

Fig. 2. Design and fabrication of GO-based milli-capsules. a) Demonstration of GO-based milli-capsules filled with drugs. b) The optical microscope image of the photo-triggered switch. c) Deformation of the photo-thermal switch serve as pressure-induced source for drug release. d) Fabrication process of the milli-capsule.
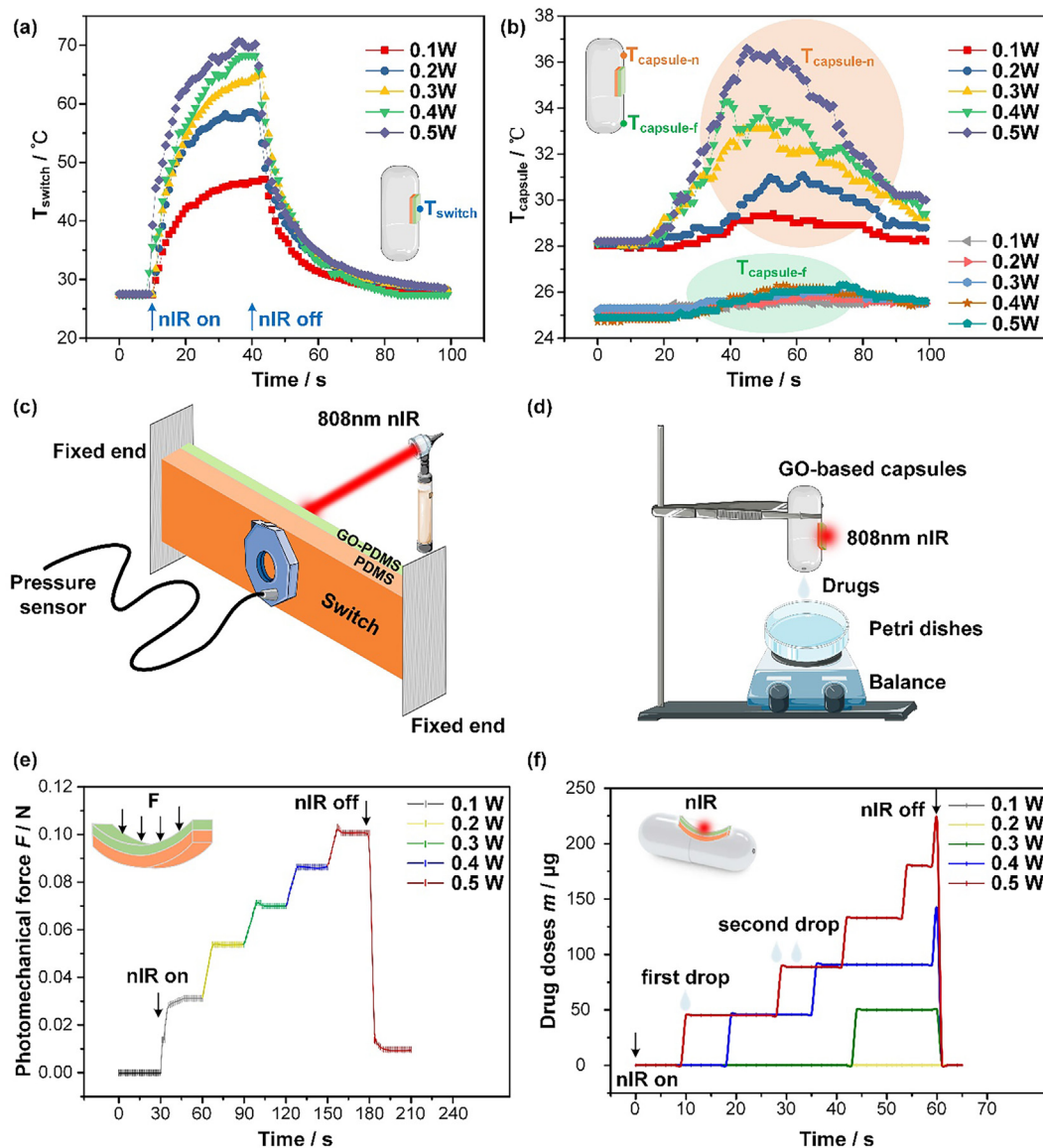
Fig. 3. The Influence of light powers on the drug-released ability. a) and b) Temperature profiles of photo-triggered switch T_{switch} and capsule-shell $T_{capsule}$ dependent on light powers and irradiating times. c) Schematic of photomechanical force testing. d) Schematic of drug dosing testing. e) Photomechanical forces for the thermal switch irradiated under different light powers. f) Dose-release relationships with different light powers.

dimensions (h and m). For the thermal properties, we have demonstrated that α decreased while E increased as the concentration of graphene oxide (w_{GO}) increased (data shown in Fig. S1), which means the thermal expansion of the upper layer is smaller than that of the bottom layer (i.e. $\alpha_{GO-PDMS} < \alpha_{PDMS}$), while the elastic modulus of the upper layer is larger than that of the bottom layer (i.e. $E_{GO-PDMS} > E_{PDMS}$, $n \geq 1$). Therefore, the two-layer planar composite film could deflect toward the GO-PDMS side, this downward deformation gives rise to the compression which pressurized on the drug reservoir and then drive drugs displacement, as Fig. 2c and Supporting Information II shows. For the structural dimensions, when $n \geq 1$, m between 0 and 1 (i.e. $h_{GO-PDMS} < h_{PDMS}$) and thinner layers (smaller h) are preferred for vigorous compression. In this study, the thickness of the GO-PDMS layer and PDMS layer were 283 μm and 336 μm, respectively, as Fig. 2b shows.

3.2.2. Drug-released controllability for GO-based capsules

When the photo-triggered switch at pre-tighten state (10 mN) and nIR light irradiating on the central of it from GO-PDMS side,

photomechanical forces F of different light powers P_L in same irradiating time (30 s) were measured by pressure sensor as Fig. 3c shows. Due to the heat transfer rate dT/dt is positively associated with P_L, the compression F increases with P_L and reaches the peak of 108 mN at 0.5 W as Fig. 3e shows, therefore support the compression force pressurized on the drug reservoir is provided by the nIR absorption and light-thermal conversion of GO-based photo-triggered switches.

Drug doses and infusion rates are key indicators of implantable drug-delivery devices. When the GO-based capsule irradiated under different light powers, measure the drug dosage released from capsules by weighting balance, and record dosing time via stopwatch as Fig. 3d shows. The time-dependent drug doses trends of different light powers in Fig. 3f can be described as: i) Every step change represents one dose released from the capsule, every plateau between steeply ascending sections represents drugs are accumulated at the boundary of the capillary hole but not fallen from the capsule. ii) At lower light powers (P_L = 0.1 W and 0.2 W), photomechanical forces were insufficient to overcome
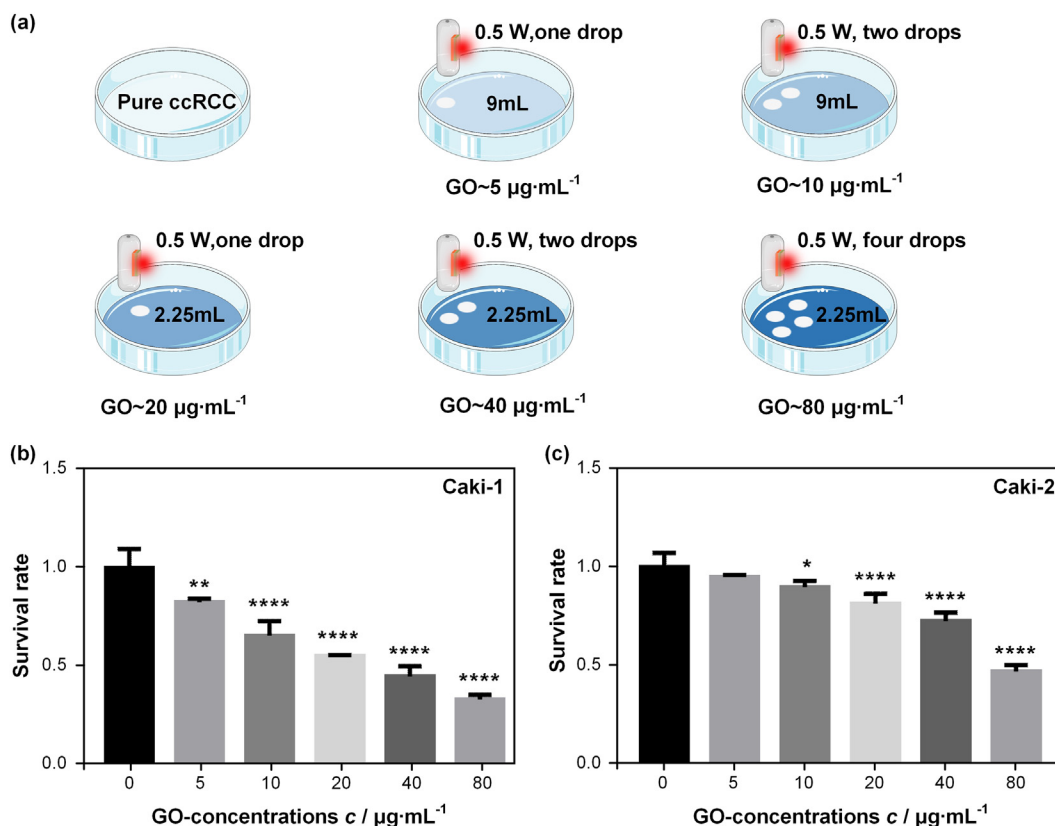
(a)

(b)

(c)

Fig. 4. Toxic Effect of Graphene Oxide on ccRCC cell viability. a) Different GO-concentrations range from 5 μg·mL^{-1} to 80 μg·mL^{-1} were achieved by capsules released various amount of GO in different volume of nutrient solution. b) and c) Toxic effects of GO on Caki-1 and Caki-2 cell lines viability. *P < 0.05, **P < 0.01 and ****P < 0.0001 compared to 0 μg·mL^{-1} group, respectively. Data are representative of three independent experiments and values are expressed in mean ± SD.

the capillary forces, and drugs were trapped in the capsule. When light powers were higher than 0.3 W, photomechanical forces were sufficient to drive drugs displacement. iii) Drug dosages and release rates increased significantly with the radiation power P_L (when P_L increased from 0.1 to 0.5 W, dosage increased from 0 μg (0 drop) to 225 μg (five drops)), and the capsule stop released when the nIR light turned off.

3.3. Cytotoxicity of graphene Oxide-based milli-capsules in vitro

3.3.1. Toxic effect of graphene oxide on ccRCC cell viability

PDMS as well-know biocompatible and nontoxic polymers have a promising perspective in implantable drug delivery,[32–35] therefore, to test the viability of GO-based milli-capsules in vivo, the cytotoxicity of GO needs further evaluated. Based on the drug release kinetics analysis in Supporting Information I, the releasable viscosity could be up to 7.41 Pa·s when capsules irradiated under 0.5 W, therefore, GO-suspensions as the drug (~10^{-4} Pa·s) embedded in capsules can be released in ccRCC environments to evaluate the toxic effect of GO. Two ccRCC cell lines (Caki-1 and Caki-2) were used to observed the cell viability, five GO-based milli-capsules filled with GO were attached to the sidewall of the petri dishes, as Fig. 4a shows.

The desired GO-concentrations c (range from 5 μg·mL^{-1} to 80 μg·mL^{-1}) in the culture dish are controlled by the drug dosage m released from capsules and volume of nutrient solution V_n, i.e. $c = c(m, V_n)$, where light powers P_L can directly influence m, i.e. $m = m(P_L)$. As Table 1 shows, when capsules irradiated under 0.5 W, $c = 5$ μg·mL^{-1} and $c = 10$ μg·mL^{-1} are obtained by capsules released one drop (45 μg) and two drops (90 μg) in 9 mL ccRCC cells, respectively. $c = 20$ μg·mL^{-1}, $c = 40$ μg·mL^{-1}L and

$c = 80$ μg·mL^{-1} are obtained by capsules released one drop (45 μg), two drops (90 μg) and four drops (180 μg) in 2.25 mL ccRCC cells, respectively.

Since ccRCC cells treated with different concentrations of GO after 48 h, using Cell Counting Kit-8 (CCK-8) assayed cell viability as Fig. 4b and c shows. When the concentrations of GO increased from 0 μg·mL^{-1} (pure ccRCC) to 80 μg·mL^{-1} (GO-ccRCC), the survival rate decreased to 33.38 % and 47.25 % for Caki-1 cell and Caki-2 cell, respectively. Thus, GO inhibits ccRCC cell proliferation in vitro and the cytotoxicity exhibits concentration-dependent manner, combined with accurate drug-dosing controllability, the GO-based milli-capsule is expected to achieve implantable ccRCC therapy.

3.3.2. Cytotoxicity assay of graphene oxide on ccRCC cell apoptosis

To investigate whether the inhibition of cell viability by GO-treatment was caused by cell apoptosis, we examined the changes of apoptotic markers in Caki-1 and Caki-2 cells after treatment with GO for 48 h. The Annexin V-FITC and propidium iodide (PI) assay revealed the significant increase in apoptosis as Fig. 5a shows. When the concentration of GO increased from 0 μg·mL^{-1} to 80 μg·mL^{-1}, the apoptotic rate of Caki-1 and Caki-2 increased to 20.70 % and 19.35 %, respectively, as Fig. 5b shows. In order to decrease test specificity, we further confirmed the apoptotic effects of GO in ccRCC cell lines by mitochondrial membrane potential (MMP) assay, which is a vital factor in the indication of early apoptosis induction.[28] JC-1 exhibits potential-dependent accumulation in mitochondria, indicated by the green fluorescence (emission at 530 ± 15 nm) for the monomers and red fluorescence (emission at 590 ± 17.5 nm) for the aggregates.
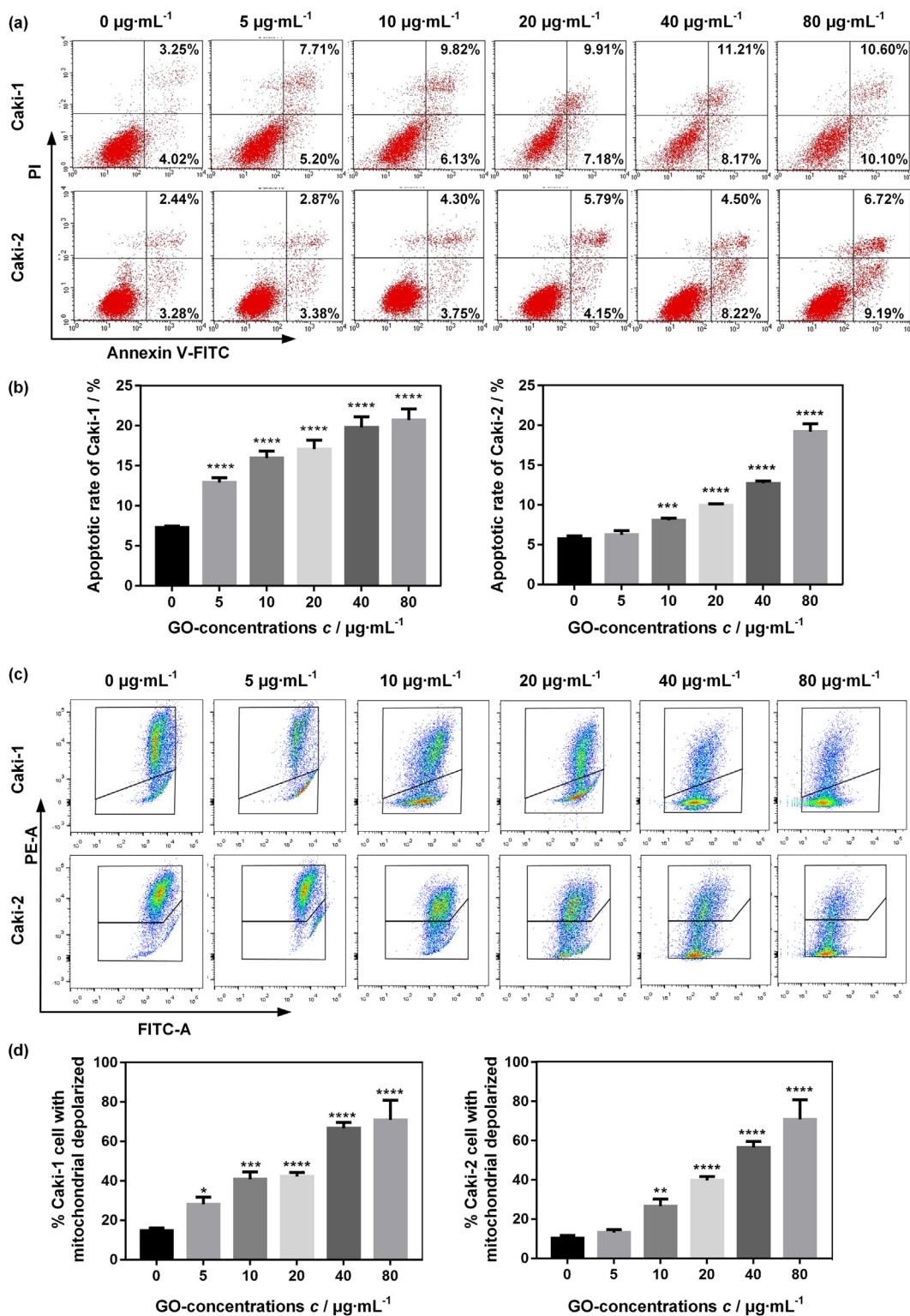
Fig. 5. GO induced apoptotic on ccRCC cell lines in a dose-dependent manner. a) Flow cytometry results with Annexin V-FITC/PI staining (Cells were treated with GO for 48 h). b) The ratio of apoptosis as the function of different GO concentrations. c) Flow cytometry results with JC-1 staining to determine changes in MMP (Cells were treated with GO for 48 h). d) The ratio of mitochondrial depolarized cells as the function of different GO concentrations. $^*P < 0.05$, $^{**}P < 0.01$, $^{***}P < 0.001$ and $^{****}P < 0.0001$ compared to 0 $\mu g \cdot mL^{-1}$ group, respectively. Data are representative of three independent experiments and values are expressed in mean ± SD.

The MMP assay reveals obvious decrease in the red/green fluorescence intensity ratio, which indicates enhanced mitochondrial depolarization, as Fig. 5c and d shows. When the concentration of GO increased from 0 $\mu g \cdot mL^{-1}$ to 80 $\mu g \cdot mL^{-1}$, the mitochondrial depolarized rate of Caki-1 and Caki-2 cells increased to 70.90 % and 66.61 %, respectively. The mitochondrial depolarized rates assayed from the MMP have been shown to correlate well with the apoptotic rates assayed from Annexin V-FITC/PI, which demonstrated
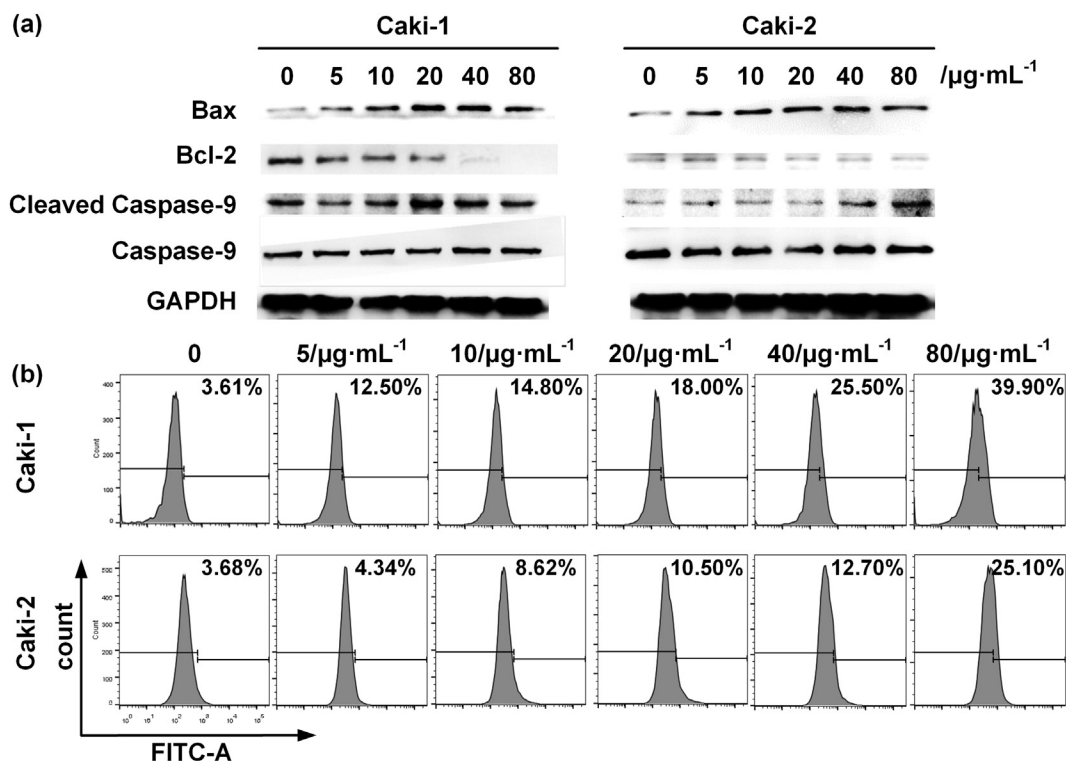
Fig. 6. GO active caspase pathway on ccRCC cell lines in a dose-dependent manner. a) Concentration-dependent expression of apoptotic proteins in GO treated ccRCC cells. b) Flow cytometric analysis of apoptotic populations for active caspase-3 with GO treatment. Data are representative of three independent experiments. ***P < 0.001 compared to untreated NSC-34 neurons.
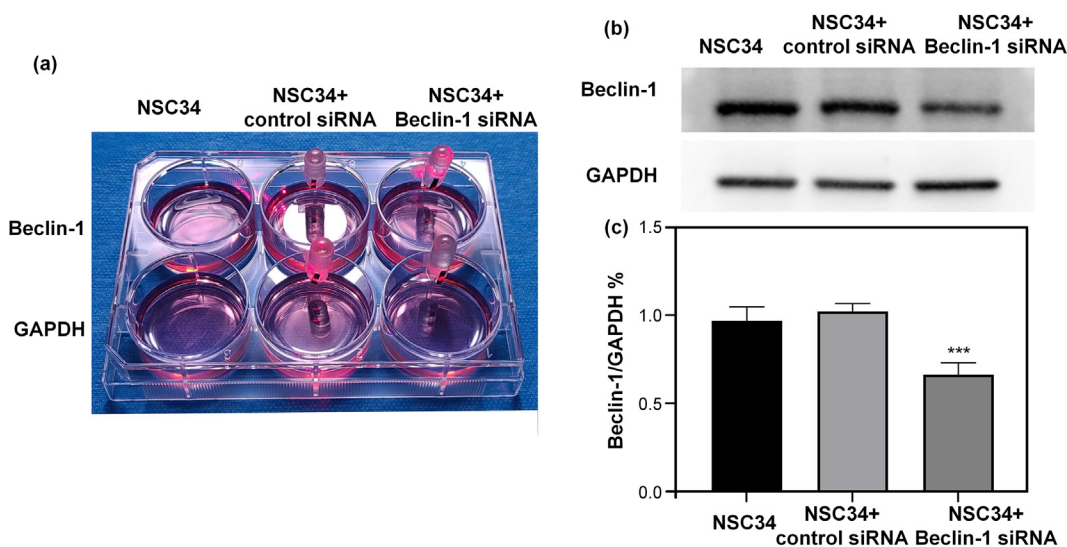

Fig. 7. siRNA-drugs embedded in GO-based milli-capsules for neurodegeneration therapy. a) NSC-34 neurons with different treatment. b) The association of Beclin-1 expression level with different transfection in NSC-34 neurons. c) siRNA-drugs' inhibition of autophagy in NSC-34 neurons. ***P < 0.001 compared to untreated NSC-34 neurons.

the inhibition of ccRCC cells viability is triggered by cell apoptosis with GO released from capsules.

Apoptotic signaling will lead to the activation of caspases, which specifically cleave native proteome substrates, leading to delocalization of proteins, loss of function or complex formation. It has been reported that caspase activation is a marker of apoptosis. [29,30] Therefore, we further evaluated the potential pathways involved in this process. The main markers of apoptosis detectible include Bax, Bcl-2, Caspase 9, Cleaved-Caspase 9, Caspase 3 and Cleaved-Caspase 3 as Fig. 6a shows. The western blot analysis demonstrated that Cleaved Caspase-9 proteins in Caki-1 and Caki-2 cells were increased as the concentration of GO increased. As Fig. 6b shows, over one third of the GO-treated Caki-1 cells were positive for active caspase-3 staining. Additionally, the expression level of Bax protein was markedly increased in a dose-dependent manner, whereas the expression level of Bcl-2 that suppressed
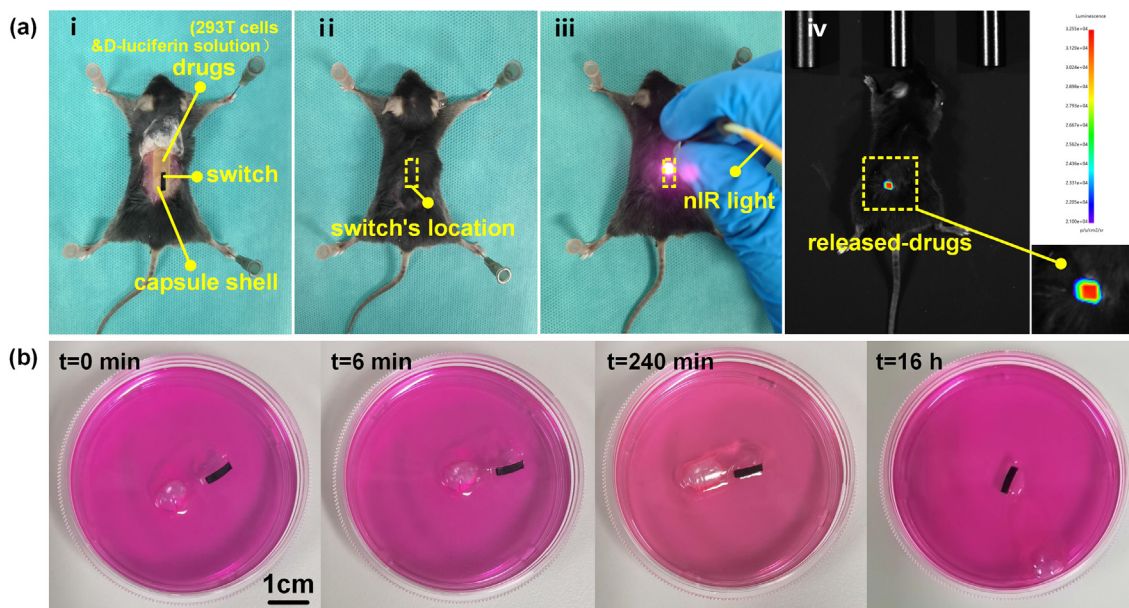
Fig. 8. a) The implantation of the milli-capsules into live mice, and the bioluminescent images to reveal the drug-release ability by remote nIR irradiation. b) Monitoring the degradation process of capsules in H-DMEM with 10% FBS solution.

apoptosis was decreased dramatically compared to GAPDH. Note that the intrinsic pathway is mainly regulated by the Bcl-2 protein family, which releases proapoptotic proteins Bax and Bak, thus, disturbs MMP to execute apoptosis signaling.

Above experiment data clearly showed that the cytotoxicity of GO could induce caspase-mediated apoptosis in ccRCC environments via the intrinsic pathway with concentration-dependent manner, which suggests the GO-based milli-capsules with accurate drug dosing ability provide a feasible path for ccRCC therapy.

3.3.3. Demonstration of GO-based milli-capsules for neurodegeneration therapy

Neurodegeneration which need to observe the progression when administrate new drugs also have an urgent request for accurate drug-dosing control. We evaluated the feasibility of GO-based milli-capsules for Neurodegeneration therapy by embedded siRNA as drugs and released in NSC-34 environments in vitro. Beclin-1, which plays an important role in neurodegeneration, is implicated in the autophagic programmed cell death. In this study, using western blot to investigate the expression of Beclin-1 after transfected by Beclin-1 or control siRNA. As Fig. 7a shows, duo to the density of GO-drugs embedded in milli-capsules is 1 µg·µL^{-1}, capsules released same volume of siRNA-drugs when irradiated under same nIR light powers, i.e. 45 µL per drop. Therefore, Beclin-1 or control siRNA transfection mixed liquid (225 µL) were achieved when capsules irradiated under 0.5 W and released five drops. As shown in Fig. 7b and c, the expression of Beclin-1 was decreased by 34.94 % compared with control siRNA group, which proved siRNA-drugs' inhibition of autophagy in NSC-34 neurons.

3.4. Performance of graphene Oxide-based milli-capsules in vivo

To further evaluate the validity of our drug delivery systems in physiological tissues, the proposed GO-based milli-capsules were implanted under the skin of live mice in vivo, as Fig. 8a shows. 293 T cells is a platform to produce viral vectors with stable over-expression of luciferase, and can be detected by ex vivo biolumi-nescence imaging when combines with D-luciferin solution. The test GO-based milli-capsule filled with 400 µL suspension of

293 T cells (1×10^6 cells) and 200 µL D-luciferin solution (25 µM) as drug was prepared before implantation. The vivo experiment in mice performed as follows: i) Female C57/BL6 mice were administrated anesthetic solution (Chloral hydrate, with suggested dose volumes 200 µL, 5 wt%) by intraperitoneal injection, after satisfactory anesthesia the mice limbs were fixed and made a skin incision (2×3 cm^2) at the side of back as the capsule's implantation site. ii) Marked switch's location, and then carefully fully closed the incision. iii) Irradiated the marked-area by nIR light ($P_L = 0.5$ W, $t = 10$ s). iv) Transfer the mice to the Multi-mode animal living imaging system within half an hour, the small animal live imaging system (Fig. 8a-iv) demonstrated that drugs (293 T cells with D-luciferin solution) had released after vitro nIR manipulation. In vivo mice experiments tested and verified the nIR lights through skin could regulate the released ability of capsules.

Furthermore, we investigate degradation of GO-based milli-capsules by immersed it (embedded with 293 T cells) into the simulated biological environment, where the nutrient solution was H-DMEM with 10 % FBS, and degradation environment was maintain at a constant temperature (37 °C) and humidity. As Fig. 8b shows, the starch capsule shell began softening after 6 min, and fully dissolved after 16 h. Although the photo-triggered switch was not dissolved, toxicity of GO and biocompability of PDMS have been respectively evaluated and proved in our study, render GO-based milli-capsules have practical use in chronic due to their refilled ability once change the capsule-shell with nonsoluble and biocompatible characteristics.

4. Conclusions

In summary, on account of near infrared light's well penetration depth through tissues and graphene oxide's light absorption ability, we developed a graphene oxide-based milli-capsules, which could realize accurate drug release by photo-induced deformation and in-vitro nIR manipulation. When the light power was 0.5 W, the photomechanical force reached to 108 mN and the dosage was up to 225 µg with five drops. The cytotoxicity of capsules in vitro was evaluated by embedded with GO as drugs and released GO in clear cell renal cell carcinoma (ccRCC) environments. When

the GO-based capsules irradiated under 0.5 W and released different amount of GO-drops in ccRCC systems, GO' concentration increased from 0 to 80 μg mL^{-1} and the proportions of apoptotic cells increased 2.85 times for Caki-1 and 2.73 times for Caki-2. The proposed GO-based milli-capsules provide accurate therapeutic strategies for ccRCC due to they can inhibit ccRCC cell proliferation in a GO-concentration-dependent manner. Replaced GO-drugs with siRNA-drugs, which perform inhibition of autophagy in NSC-34 neurons (the expression of Beclin-1 was decreased by 34.94 % compared with the control siRNA group), furnishing an additional proof of the practicability of GO-based milli-capsules for neurodegeneration therapy. The final in-vivo mice experiment further evaluated the validity of our milli-capsules applied in implantable drug delivery.

Data availability

The data that supports this study is available within the article and its supplementary data files or available from the authors upon request.

Data availability

Data will be made available on request.

Declaration of Competing Interest

The authors declare that they have no known competing financial interests or personal relationships that could have appeared to influence the work reported in this paper.

Acknowledgements

Appendix A. Supplementary material

Supplementary data to this article can be found online at https://doi.org/10.1016/j.matdes.2022.111287.

References

[1] J.J. Hsieh, M.P. Purdue, S. Signoretti, C. Swanton, L. Albiges, M. Schmidinger, D.Y. Heng, J. Larkin, V. Ficarra, Renal cell carcinoma, Nat. Rev. Dis. Primers. 3 (1) (2017) 1–19, https://doi.org/10.1038/nrdp.2017.9.

[2] H.T. Cohen, F.J. McGovern, Renal-cell carcinoma, N. Engl. J. Med. 353 (23) (2005) 2477–2490, https://doi.org/10.1056/NEJMra043172.

[3] R.L. Siegel, K.D. Miller, H.E. Fuchs, A. Jemal, Cancer statistics, 2022, Ca-Cancer J. Clin. (2022), https://doi.org/10.3322/caac.21708.

[4] J.S. Lam, O. Shvarts, J.T. Leppert, A.J. Pantuck, R.A. Figlin, A.S. Belldegrun, Postoperative surveillance protocol for patients with localized and locally advanced renal cell carcinoma based on a validated prognostic nomogram and risk group stratification system, J. Urol. 174 (2) (2005) 466–472, https://doi.org/10.1097/01.ju.0000165572.38887.da.

[5] K. Gupta, J.D. Miller, J.Z. Li, M.W. Russell, C. Charbonneau, Epidemiologic and socioeconomic burden of metastatic renal cell carcinoma (mRCC): a literature review, Cancer Treat. Rev. 34 (3) (2008) 193–205, https://doi.org/10.1016/j.ctrv.2007.12.001.

[6] S.C. Joosten, I.A. Deckers, M.J. Aarts, A. Hoeben, J.G. van Roermund, K.M. Smits, V. Melotte, M. van Engeland, V.C. Tjan-Heijnen, Prognostic DNA methylation markers for renal cell carcinoma: a systematic review, Epigenomics 9 (9) (2017) 1243–1257, https://doi.org/10.2217/epi-2017-0040.

[7] L.B. Tovar-y-Romo, L.D. Santa-Cruz, R. Tapia, Experimental models for the study of neurodegeneration in amyotrophic lateral sclerosis, Mol. Neurodegener. 4 (1) (2009) 1–13, https://doi.org/10.1186/1750-1326-4-31.

[8] E.M. Posadas, S. Limvorasak, R.A. Figlin, Targeted therapies for renal cell carcinoma, Nat. Rev. Nephrol. 13 (8) (2017) 496–511, https://doi.org/10.1038/nrneph.2017.82.

[9] K. Zarrabi, S. Wu, Current and emerging therapeutic targets for metastatic renal cell carcinoma, Curr. Oncol. Rep. 20 (5) (2018) 1–14, https://doi.org/10.1007/s11912-018-0684-z.

[10] A. Rodriguez-Vida, T.E. Hutson, J. Bellmunt, M.H. Strijbos, New treatment options for metastatic renal cell carcinoma, ESMO open 2 (2) (2017) e000185.

[11] P.C. Barata, B.I. Rini, Treatment of renal cell carcinoma: current status and future directions, Ca-Cancer J. Clin. 67 (6) (2017) 507–524, https://doi.org/10.3322/caac.21411.

[12] B. Li, H. Tan, D. Jenkins, V.S. Raghavan, B.G. Rosa, F. Güder, G. Pan, E. Yeatman, D.J. Sharp, Clinical detection of neurodegenerative blood biomarkers using graphene immunosensor, Carbon 168 (2020) 144–162, https://doi.org/10.1016/j.carbon.2020.06.048.

[13] X. Cui, S. Xu, X. Wang, C. Chen, The nano-bio interaction and biomedical applications of carbon nanomaterials, Carbon 138 (2018) 436–450, https://doi.org/10.1016/j.carbon.2018.07.069.

[14] M. Burnett, Y. Abuetabh, A. Wronski, F. Shen, S. Persad, R. Leng, D. Eisenstat, C. Sergi, Graphene oxide nanoparticles induce apoptosis in wild-type and CRISPR/Cas9-IGF/IGFBP3 knocked-out osteosarcoma cells, J. Cancer. 11 (17) (2020) 5007, https://doi.org/10.7150/jca.46464.

[15] T. Kavinkumar, K. Varunkumar, V. Ravikumar, S. Manivannan, Anticancer activity of graphene oxide-reduced graphene oxide-silver nanoparticle composites, J. Colloid Interface Sci. 505 (2017) 1125–1133, https://doi.org/10.1016/j.jcis.2017.07.002.

[16] F. Yaghoubi, N.S.H. Motlagh, S.M. Naghib, F. Haghiralsadat, H.Z. Jaliani, A. Moradi, A functionalized graphene oxide with improved cytocompatibility for stimuli-responsive co-delivery of curcumin and doxorubicin in cancer treatment, Sci. Rep. 12 (1) (2022) 1–18, https://doi.org/10.1038/s41598-022-05793-9.

[17] A. Paul, A. Hasan, H.A. Kindi, A.K. Gaharwar, V.T. Rao, M. Nikkhah, S.R. Shin, D. Krafft, M.R. Dokmeci, D. Shum-Tim, Injectable graphene oxide/hydrogel-based angiogenic gene delivery system for vasculogenesis and cardiac repair, ACS nano 8 (8) (2014) 8050–8062, https://doi.org/10.1021/nn5020787.

[18] J. Park, B. Kim, J. Han, J. Oh, S. Park, S. Ryu, S. Jung, J.-Y. Shin, B.S. Lee, B.H. Hong, Graphene oxide flakes as a cellular adhesive: prevention of reactive oxygen species mediated death of implanted cells for cardiac repair, ACS nano 9 (5) (2015) 4987–4999, https://doi.org/10.1021/nn507149w.

[19] Y. Piao, B. Chen, Self-assembled graphene oxide–gelatin nanocomposite hydrogels: characterization, formation mechanisms, and pH-sensitive drug release behavior, J. Polym. Sci., Part B: Polym. Phys. 53 (5) (2015) 356–367, https://doi.org/10.1002/polb.23636.

[20] S. Adepu, S. Ramakrishna, Controlled drug delivery systems: current status and future directions, Molecules 26 (19) (2021) 5905, https://doi.org/10.3390/molecules26195905.

[21] A. Hardenia, N. Maheshwari, S.S. Hardenia, S.K. Dwivedi, R. Maheshwari, R.K. Tekade, 2019. Scientific rationale for designing controlled drug delivery systems, Basic Fundamentals of Drug Delivery. Elsevier. pp. 1–28. 10.1016/B978-0-12-817909-3.00001-7.

[22] K. Park, Controlled drug delivery systems: past forward and future back, J. Controlled Release 190 (2014) 3–8, https://doi.org/10.1016/j.jconrel.2014.03.054.

[23] E. Meng, T. Hoang, Micro-and nano-fabricated implantable drug-delivery systems, Ther. Delivery. 3 (12) (2012) 1457–1467, https://doi.org/10.4155/tde.12.132.

[24] T. Marín, P. Montoya, O. Arnache, R. Pinal, J. Calderón, Development of magnetite nanoparticles/gelatin composite films for triggering drug release by an external magnetic field, Mater. Des. 152 (2018) 78–87, https://doi.org/10.1016/j.matdes.2018.04.073.

[25] S.S. Park, M.H. Jung, Y.-S. Lee, J.-H. Bae, S.-H. Kim, C.-S. Ha, Functionalised mesoporous silica nanoparticles with excellent cytotoxicity against various cancer cells for pH-responsive and controlled drug delivery, Mater. Des. 184 (2019), https://doi.org/10.1016/j.matdes.2019.108187 108187.

[26] T. Kubota, Y. Kurashina, J. Zhao, K. Ando, H. Onoe, Ultrasound-triggered on-demand drug delivery using hydrogel microbeads with release enhancer, Mater. Des. 203 (2021), https://doi.org/10.1016/j.matdes.2021.109580 109580.

[27] C.-C. Weng, T.-A. Yang, Y.-K. Li, Design and fabrication of cell-targeted, dual drug-loaded nanoparticles with pH-controlled drug release and near-infrared light-induced photothermal effects, Mater. Des. 197 (2021), https://doi.org/10.1016/j.matdes.2020.109230 109230.

[28] S. De Biasi, L. Gibellini, A. Cossarizza, Uncompensated polychromatic analysis of mitochondrial membrane potential using JC-1 and multilaser excitation, Curr. Protoc. Cytom. 72(1) (2015) 7.32. 1-7.32. 11. 10.1002/0471142956.cy0732s72.

[29] J. Grosse, E. Warnke, M. Wehland, J. Pietsch, F. Pohl, P. Wise, N.E. Magnusson, C. Eilles, D. Grimm, Mechanisms of apoptosis in irradiated and sunitinib-treated follicular thyroid cancer cells, Apoptosis 19 (3) (2014) 480–490, https://doi.org/10.1007/s10495-013-0937-0.

[30] D.N. Martin, E.H. Baehrecke, Caspases function in autophagic programmed cell death in Drosophila, Development 131 (2) (2004) 275–284.

[31] M. Karimi, A. Ghasemi, P. Sahandi Zangabad, R. Rahighi, S.M. Moosavi Basri, H. Mirshekari, M. Amiri, Z. Shafaei Pishabad, A. Aslani, M. Bozorgomid, D. Ghosh, A. Beyzavi, A. Vaseghi, A.R. Aref, L. Haghani, S. Bahrami, M.R. Hamblin, Smart

micro/nanoparticles in stimulus-responsive drug/gene delivery systems, Chem. Soc. Rev. 45 (5) (2016) 1457–1501.

[32] M.C. Bélanger, Y. Marois, Hemocompatibility, biocompatibility, inflammatory and in vivo studies of primary reference materials low-density polyethylene and polydimethylsiloxane: A review, J. Biomed. Mater. Res., Part B 58 (5) (2001) 467–477, https://doi.org/10.1002/jbm.1043.

[33] H. Wu, J. Zhu, Y. Huang, D. Wu, J. Sun, Microfluidic-based single-cell study: current status and future perspective, Molecules 23 (9) (2018) 2347, https://doi.org/10.3390/molecules23092347.

[34] D. Wang, D. Ba, Z. Hao, Y. Li, F. Sun, K. Liu, G. Du, Q. Mei, A novel approach for PDMS thin films production towards application as substrate for flexible biosensors, Mater. Lett. 221 (2018) 228–231, https://doi.org/10.1016/j.matlet.2018.03.114.

[35] H. Liu, R. Jian, H. Chen, X. Tian, C. Sun, J. Zhu, Z. Yang, J. Sun, C. Wang, Application of biodegradable and biocompatible nanocomposites in electronics: current status and future directions, Nanomaterials 9 (7) (2019) 950, https://doi.org/10.3390/nano9070950.

[36] A. Mohapatra, S. Uthaman, I.-K. Park, Polyethylene glycol nanoparticles as promising tools for anticancer therapeutics, Polym. Nanopart. Promising Tool Anti-Cancer Ther. (2019) 205–231, https://doi.org/10.1016/B978-0-12-816963-6.00010-8.

[37] P.-Y. Li, T.K. Givrad, R. Sheybani, D.P. Holschneider, J.-M.-I. Maarek, E. Meng, A low power, on demand electrothermal valve for wireless drug delivery applications, Lab Chip. 10 (1) (2010) 101–110, https://doi.org/10.1039/B910248E.

[38] S. Rahimi, E.H. Sarraf, G.K. Wong, K. Takahata, Implantable drug delivery device using frequency-controlled wireless hydrogel microvalves, Biomed. Microdevices 13 (2) (2011) 267–277, https://doi.org/10.1007/s10544-010-9491-5.

[39] T. Tagami, W.D. Foltz, M.J. Ernsting, C.M. Lee, I.F. Tannock, J.P. May, S.-D. Li, MRI monitoring of intratumoral drug delivery and prediction of the therapeutic effect with a multifunctional thermosensitive liposome, Biomaterials 32 (27) (2011) 6570–6578, https://doi.org/10.1016/j.biomaterials.2011.05.029.

[40] S. Mura, J. Nicolas, P. Couvreur, Stimuli-responsive nanocarriers for drug delivery, Nat. Mater. 12 (11) (2013) 991–1003, https://doi.org/10.1038/nmat3776.

[41] F.N. Pirmoradi, J.K. Jackson, H.M. Burt, M. Chiao, On-demand controlled release of docetaxel from a battery-less MEMS drug delivery device, Lab Chip. 11 (16) (2011) 2744–2752, https://doi.org/10.1039/C1LC20134D.

[42] F.F. Sahle, M. Gulfam, T.L. Lowe, Design strategies for physical-stimuli-responsive programmable nanotherapeutics, Drug Discovery Today 23 (5) (2018) 992–1006, https://doi.org/10.1016/j.drudis.2018.04.003.

[43] L. Wu, J. Wang, N. Gao, J. Ren, A. Zhao, X. Qu, Electrically pulsatile responsive drug delivery platform for treatment of Alzheimer's disease, Nano Res. 8 (7) (2015) 2400–2414, https://doi.org/10.1007/s12274-015-0750-x.

[44] M.A. Rahim, N. Jan, S. Khan, H. Shah, A. Madni, A. Khan, A. Jabar, S. Khan, A. Elhissi, Z. Hussain, Recent advancements in stimuli responsive drug delivery platforms for active and passive cancer targeting, Cancers 13 (4) (2021) 670, https://doi.org/10.3390/cancers13040670.

[45] Y. Lu, W. Sun, Z. Gu, Stimuli-responsive nanomaterials for therapeutic protein delivery, J. Controlled Release 194 (2014) 1–19, https://doi.org/10.1016/j.jconrel.2014.08.015.